Chaotic mixing via streamline jumping in quasi-two-dimensional tumbled granular flows

Ivan C. Christov,[1,a)] Julio M. Ottino,[2,3,4,b)] and Richard M. Lueptow[4,c)]
[1]*Department of Engineering Sciences and Applied Mathematics, Northwestern University, Evanston, Illinois 60208, USA*
[2]*Department of Chemical and Biological Engineering, Northwestern University, Evanston, Illinois 60208, USA*
[3]*The Northwestern Institute on Complex Systems (NICO), Northwestern University, Evanston, Illinois 60208, USA*
[4]*Department of Mechanical Engineering, Northwestern University, Evanston, Illinois 60208, USA*

(Received 23 October 2009; accepted 1 March 2010; published online 19 April 2010)

We study, numerically and analytically, the singular limit of a vanishing flowing layer in tumbled granular flows in quasi-two-dimensional rotating containers. The limiting behavior is found to be identical under the two versions of the kinematic continuum model of such flows, and the transition to the limiting dynamics is analyzed in detail. In particular, we formulate the no-shear-layer dynamical system as a piecewise isometry. It is shown how such a discontinuous map, through the concordant mechanism of streamline jumping, leads to the physical mixing of granular matter. The dependence of the dynamics of Lagrangian particle trajectories on the tumbler fill fraction is also established through Poincaré sections, and, in the special case of a half-full tumbler, chaotic behavior is shown to disappear completely in the singular limit. At other fill levels, stretching in the sense of shear strain is replaced by spreading due to streamline jumping. Finally, we use finite-time Lyapunov exponents to establish the manifold structure and understand "how chaotic" the limiting piecewise isometry is. © *2010 American Institute of Physics*. [doi:10.1063/1.3368695]

A successful approach to studying mixing in granular flows is based on chaotic advection. Numerous studies have shown that the mixing and segregation of tumbled particulate matter is to a large extent controlled by the shape of the container and can be related to the Poincaré section for a kinematic model of the flow. While fluid mixing is fundamentally about modulating the flow so that particles can switch between different streamlines, granular flows appear to exhibit a related, but fundamentally different, behavior, namely, that particles can discontinuously jump between streamlines. This is possible because tumbled granular flows consist of a thin flowing layer above a fixed bed of particles, meaning it is physically possible to make the region of streamline crossing arbitrarily small—a classical singular perturbation problem. Even though the limiting dynamics do not possess the same stretching characteristics as chaotic flows, they can nevertheless lead to the successful, and seemingly chaotic, mixing of granular matter in a tumbler.

I. INTRODUCTION

The study of the stability of fixed and periodic points in flows (both physical and mathematical) is one of the cornerstones of *deterministic chaos*.[1,2] Among the various tools available to investigate periodic points, and determine "how chaotic" a flow is, none is more revealing and visually appealing than the *Poincaré section*. Although strictly speaking only applicable to flows with built-in periodicity (spatial, temporal, or both), this stroboscopic map captures the location of a "particle" (used here in the most general sense) at a uniform sequence of instants of time (i.e., multiples of the underlying flow's period) as it is advected by the flow. In the study of mixing of fluids in particular, Poincaré sections have become a type of visual guide that immediately shows where to expect "good" and "bad" mixing in a given flow.[3,4] In the study of mixing of granular matter (e.g., powders, grains, and sands), on the other hand, there is a surprising connection between the Poincaré section and the antithesis of mixing: the *segregation* of bidisperse particles.[5,6] What is more, the Poincaré section has proven to be a useful tool for analyzing experimental data (e.g., from mixing studies[7] or motion of diamagnetic particles[8]) and in the theory of collective granular dynamics (e.g., of sheared packings[9] or vibrated beds[10]), to name a few.

The utility of the Poincaré section lies in its ability to visualize the "islands," i.e., regions indicative of "poor" mixing and potential segregation.[11] Here, we should note that while a Poincaré section is completely determined once the flow (in the sense of a dynamical system or in the sense of physical motion) is given, there is a significant difference between the two types of granular mixing experiments it can be used in, namely, *monodisperse* and *bidisperse*. For monodisperse granular matter, regions of mixing of particles of

[a)]Electronic mail: christov@u.northwestern.edu. URL: http://alum.mit.edu/www/christov.
[b)]Electronic mail: jm-ottino@northwestern.edu. URL: http://mixing.chem-eng.northwestern.edu.
[c)]Author to whom correspondence should be addressed. Electronic mail: r-lueptow@northwestern.edu. URL: http://www.mech.northwestern.edu/lueptow.

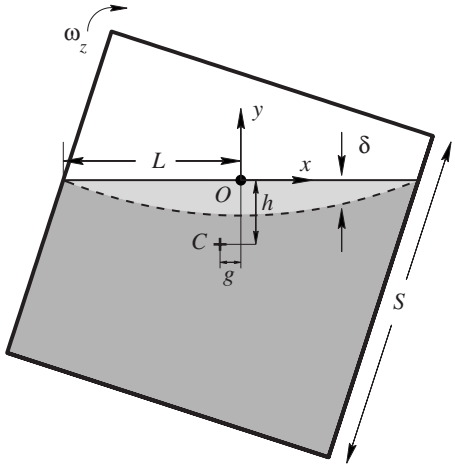

FIG. 1. Diagram of a 70% full square quasi-two-dimensional tumbler, which has been rotated backward by the dynamic angle of repose so the surface of the flowing layer is horizontal, showing the coordinate system and notation. The thickness of the tumbler is assumed much smaller than its width and height, so it is not shown. The boundary of the flowing layer is represented by a dashed curve.

different colors (for example) is predicted by the Poincaré section; for bidisperse granular matter, the segregation pattern (due to either particle density or size differences) is predicted.

Recently, *finite-time* Lagrangian transport analysis,[12,13] through the concept of a finite-time Lyapunov exponent (FTLE), has proven to be a tool that is as useful as the Poincaré section for studying mixing in general (i.e., not necessarily periodic) nonautonomous dynamical systems. Since the usual asymptotic definitions of dynamical systems theory are not well suited for characterizing transient behavior, this has led to the development of the concept of a *Lagrangian coherent structure* (LCS).[14,15] These analogs of separatrices and manifolds can be determined from a finite number of particle trajectories, even experimentally obtained ones.[16] Thus, LCSs provide a simple way of identifying the manifold structure associated with (hyperbolic) periodic points, which has also been shown to characterize segregation patterns,[6] in tumbled granular flows without the need to even locate the periodic points.

Making heavy use of Poincaré sections to capture the time-periodic behavior and LCSs to identify the manifold structure of the underlying flows, in the present work, we focus purely on the kinematics of motion in what is known as a *tumbled granular flow*, i.e., the motion of particles in a convex (for our purposes) quasi-two-dimensional (meaning thickness is negligible compared with height and width) container. The granular matter in the container is assumed to fill a certain fraction ϕ of the available volume and to be in the *continuous flow*[17] regime, i.e., the regime where some of the particles are continuously flowing down a thin lens-shaped *fluidized (shear) layer*[18] at the free surface, while the rest are in solid body rotation with the container. Moreover, it is assumed that this process is not fast enough to deform the free surface to the point where it is no longer flat. All these assumptions and the geometry are illustrated in Fig. 1 for an example square tumbler.

In particular, we are interested in the dynamics of Lagrangian (particle) trajectories under this mathematical model as the shear layer becomes vanishingly thin. We wish to establish whether chaotic, or otherwise complicated, dynamics can persist if the flowing layer has zero thickness, and we wish to establish precisely how the transition to the limiting behavior occurs. In contrast with the earlier mathematical analysis[19] of the limiting case, we show how the limiting dynamical system emerges from the kinematic model of tumbled granular flow and study the transition to this state.

The effects of a vanishing flowing layer thickness are also briefly explored elsewhere for a quasi-two-dimensional square[20] and more completely for a half-full three-dimensional spherical tumbler.[21,22] In two dimensions, *streamline jumping* leads to complicated particle trajectories, while *cutting and shuffling* leads to mixing in three dimensions. In both cases, an unexpected connection is with *piecewise isometries*,[23,24] an emergent branch of dynamical systems theory. Much like how *linked twist maps* are the fundamental underlying feature of good fluid mixing,[25] it appears that piecewise isometries are the roadmap to mixing in tumbled granular flows.

Here, we present an in-depth study based on detailed numerical simulations of the governing dynamical system and show that the dynamics of particle trajectories are nontrivial and quite complex, which we quantify using FTLE calculations. The effect of the fill fraction on the limit is also established, showing the hallmarks of a classical *singular perturbation*.

II. A CONTINUUM MODEL OF TUMBLED GRANULAR FLOW

A number of continuum models (i.e., models that replace the discrete effects of particle interactions with a continuous macroscopic medium possessing certain stress-strain relations, etc.) exist in the literature. Some focus on the phenomenology of axial segregation[26,27] leading to a system of nonlinear partial differential equations, while others focus on the kinematics of the flow[28,29] giving rise to finite-dimensional nonlinear dynamical systems (i.e., ordinary differential equations). Geometric models play an important role in three dimensions: the flow can be treated in terms of the angles of rotation of the tumbler[30] or a variational formulation based on energy conservation.[31] Modeling the rheology[32,33] and the resulting mass, momentum, and energy conservation partial differential equations[34,35] of the "granular continuum" has also received much attention. Yet this is just the beginning of the list, for which more details can be found in recent reviews on the topic.[36,37]

Focusing on the situation illustrated in Fig. 1, it is clear that the governing equations of the motion must be piecewise defined. First, near the free surface of the flow, there is the *flowing layer* (i.e., the thin lens-shaped light gray region of shear in Fig. 1). Second, below the flowing layer, there is the *bulk* or *fixed bed* (i.e., the dark gray region in Fig. 1) of particles that are in solid body rotation. To express this mathematically, let $\hat{\boldsymbol{i}}$, $\hat{\boldsymbol{j}}$, and $\hat{\boldsymbol{k}}$ denote the unit vectors in the x, y,

and z coordinate directions, respectively, which are defined with respect to the midpoint of the flowing layer O. Analogously, we can define the coordinates $\tilde{x}$, $\tilde{y}$, and $\tilde{z}$ with respect to the center of rotation of the tumbler C. In this notation, the angular velocity of the container is $\boldsymbol{\omega}=\omega_z\hat{\boldsymbol{k}}$.

Following the kinematic approach to advection,[4,38] if we let $\boldsymbol{r}(t)=x(t)\hat{\boldsymbol{i}}+y(t)\hat{\boldsymbol{j}}$ be a *pathline* (i.e., a Lagrangian trajectory of a particle) in this tumbled flow, then the dynamic equations of its evolution in the moving frame are

$$\frac{\mathrm{d}}{\mathrm{d}t}x(t)=\begin{cases} v_x(x(t),y(t),t), & y(t) > -\delta(x(t),t), \\ \omega_z[y(t)+h(t)]-\dot{g}(t), & \text{otherwise}, \end{cases} \tag{1a}$$

$$\frac{\mathrm{d}}{\mathrm{d}t}y(t)=\begin{cases} v_y(x(t),y(t),t), & y(t) > -\delta(x(t),t), \\ -\omega_z[x(t)+g(t)]-\dot{h}(t), & \text{otherwise}, \end{cases} \tag{1b}$$

where $(v_x,v_y)^{\mathsf{T}}$ is the Eulerian velocity field in the flowing layer, a superimposed dot indicates a time derivative, and $\omega_z(>0)$ is the *clockwise* rotation rate. Although simple to write, this is a rather intricate dynamical system, as the interface between the two cases on the right-hand side moves in space with time; its motion is solely determined by the tumbler shape, so it is known *a priori*.

In particular, it is generally the case that

$$v_x(x,-\delta(x,t),t) \neq \omega_z[-\delta(x,t)+h(t)]-\dot{g}(t), \tag{2a}$$

$$v_y(x,-\delta(x,t),t) \neq -\omega_z[x+g(t)]-\dot{h}(t). \tag{2b}$$

Although, as far as the physics is concerned, this is not an issue,[36] this discontinuity qualifies Eq. (1), mathematically, as a *nonsmooth*[39] or *Filippov-type*[40] dynamical system, with a *discontinuity boundary* (also know as *switching manifold*) given by $y=-\delta(x,t)$. Simply put, this means that a number of mathematical techniques for studying nonlinear dynamics[1,2] do not directly apply to such systems, which makes the analysis quite challenging, especially with regard to bifurcation theory.[40] Fortunately, some "classical" results for smooth dynamical systems, such as the Kolmogorov–Arnold–Moser (KAM) theorem,[2,3] carry over.[39] As a result, qualitative methods and numerical simulation of the governing equation are a fruitful approach to studying the vanishing flowing layer limit.

Below, we cover the two choices for the flowing-layer velocity field $(v_x,v_y)^{\mathsf{T}}$ found in the literature, both of which presume that the streamwise velocity component v_x varies linearly with the depth y in the flowing layer, a result based on a first approximation to the experimentally obtained velocity profile.[41,42] Then, the transverse component v_y is found by invoking mass conservation for a homogeneous incompressible continuum.[11,28,29,36] The model assumes a simple rheology as a first approximation of the experimental results,[28,29,41,42] although granular flows can exhibit a great variety of rheological properties depending on the type of deformation.[43,44]

At this point, the paradigm of *chaotic advection*,[4,38] or *Lagrangian chaos*, is typically applied to tumbled granular flows. Its essence lies in the realization that the kinematic continuum model satisfies[11,29] the (heuristic) sufficient condition for chaotic mixing, namely, *streamline crossing*[4]—an idea that has been formalized mathematically using linked twist maps.[25] This refers to the fact that if we were to superimpose the streamlines of the velocity field [i.e., the right-hand sides of Eq. (1)] at two close but distinct times, say at t and $t+\Delta t$, then we would see intersecting streamlines. Figure 2 illustrates this for two different tumbler cross sections in which streamline crossing occurs as a consequence of the changing length and thickness of the flowing layer. It is also possible to create streamline crossing in tumbled granular flows in circular containers, where the flowing layer's length and depth remain fixed, by varying the rotation rate in time.[45] Finally, we note that other complementary ways to characterize mixing *a priori* have been developed recently, such as the notion of *transversely oriented shears*.[46]

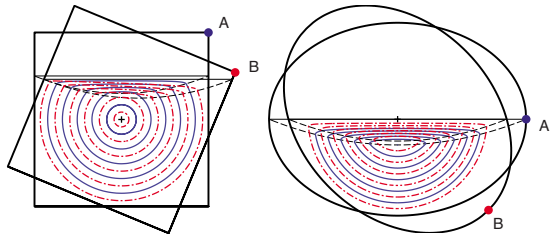

(a) 75% full square tumbler (b) 50% full elliptic tumbler

FIG. 2. (Color online) Illustration of streamline crossing in two tumbler geometries. Solid (blue) and dot-dashed (red) streamlines correspond to the flow when the tumbler is in orientations A and B, respectively. Note that they cross in the region where the flowing layers of the two orientations overlap, but they do not cross in the bulk. Orientation B is orientation A rotated (a) 22.5° and (b) 45° clockwise.

A. Depth-averaged streamwise velocity does not vary with position

Under the original model of Khakhar *et al.*,[29] which we refer to by an A superscript, omitting the effects of diffusion due to interparticle collisions, the velocity field in the flowing layer takes the form

$$v_x^A(x,y,t)=2\bar{v}_x(t)[1+y/\delta^A(x,t)], \tag{3a}$$

$$v_y^A(x,y,t)=-\omega_z x[y/\delta^A(x,t)]^2, \tag{3b}$$

where

$$\delta^A(x,t)=\delta_0(t)\left\{1-\left[\frac{x}{L(t)}\right]^2\right\}, \quad \bar{v}_x(t)=\frac{\omega_z L(t)^2}{2\delta_0(t)} \tag{4}$$

are the shape of the flowing layer and the depth-averaged streamwise velocity in the flowing layer, respectively.

Here, the maximal depth of the flowing layer $\delta_0(t)$ and the half-length of the free surface $L(t)$ are known functions of time alone and are such that $\epsilon:=\delta_0(t)/L(t)$ can be assumed to be a constant independent of time.[11,29] This experimentally motivated the assumption that $\epsilon=\text{const}$ is termed the *geometric similarity* of the flowing layer because, physically, it means that the flowing layer adjusts instantaneously to changes in the container's orientation, for instance, when it intersects a corner. Moreover, experiments[41,42] have shown that the maximal flowing layer depth δ_0 is typically 5–12

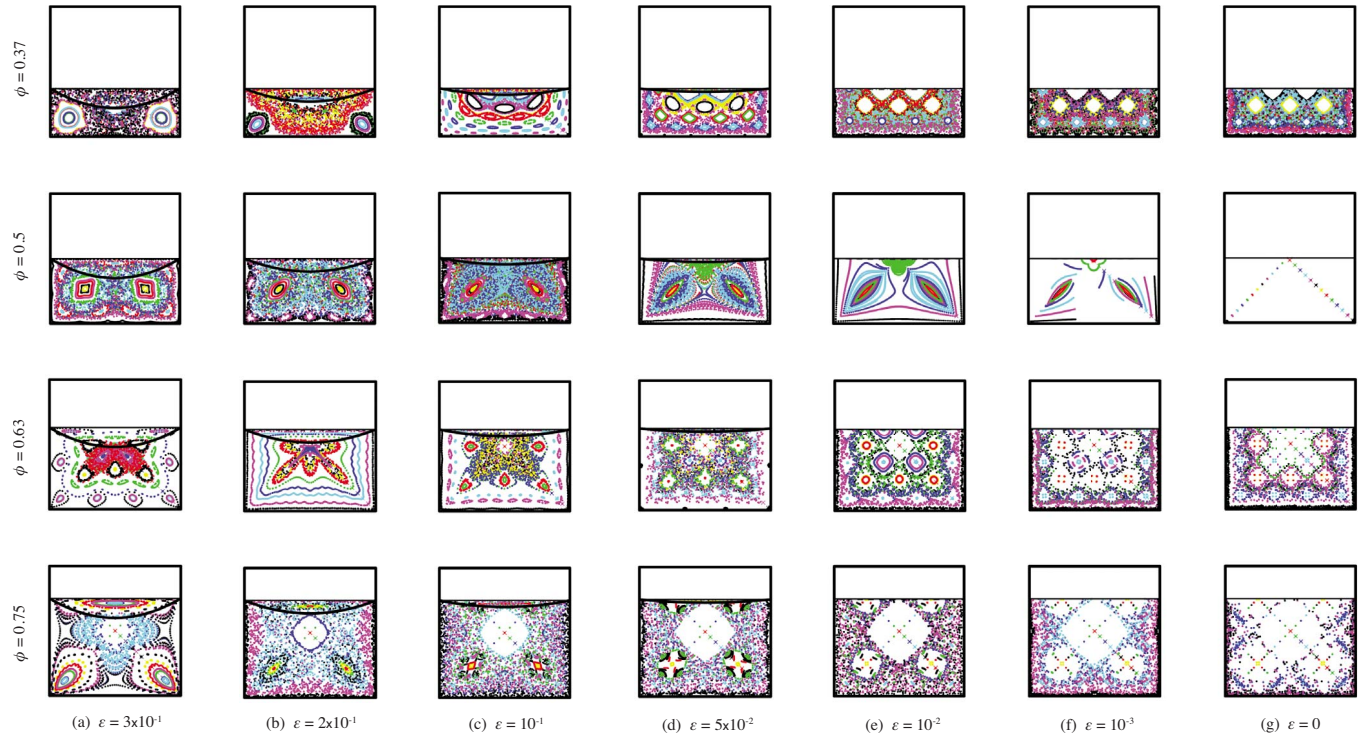

FIG. 3. (Color online) Evolution of the 500-period Poincaré section of the tumbled granular flow in (ϕ,ϵ) phase space as ϕ increases (from top to bottom) and ϵ decreases (from left to right). In each plot, the different shades correspond to different initial positions of the advected tracer particles (see Appendix), and the thick curves correspond to the flowing layer boundary $y=-\delta(x,0)$.

particle diameters, which is much smaller than the length of the free surface $2L$, so $\epsilon \ll 1$.

Now, we introduce the dimensionless variables

$$x^\star = x/\ell, \quad y^\star = y/\ell, \quad L^\star = L/\ell,$$
$$\delta_0^\star = \delta_0/\ell, \quad t^\star = \omega_z t, \quad v^\star = v/(\ell\omega_z), \tag{5}$$

where ℓ is some reference length, e.g., a square tumbler's side-length S. Then, upon substituting the relations in Eq. (4) into Eq. (3), switching to the dimensionless variables, and leaving all star superscripts understood we obtain

$$v_x^A(x,y,t) = \frac{L}{\epsilon^2}\left(\epsilon + \frac{yL}{L^2-x^2}\right), \tag{6a}$$

$$v_y^A(x,y,t) = -\frac{x}{\epsilon^2}\left(\frac{yL}{L^2-x^2}\right)^2. \tag{6b}$$

B. Simple shear rate is constant

Under the constant-simple-shear model of Makse[47] (see also the discussion by Meier *et al.*[36]), which we refer to by a B superscript, the velocity field in the flowing layer is

$$v_x^B(x,y,t) = \dot\gamma\delta^B(x,t)[1 + y/\delta^B(x,t)], \tag{7a}$$

$$v_y^B(x,y,t) = \omega_z xy/\delta^B(x,t), \tag{7b}$$

where

$$\delta^B(x,t) = \delta_0(t)\sqrt{1-\left[\frac{x}{L(t)}\right]^2}, \quad \dot\gamma = \omega_z\left[\frac{L(t)}{\delta_0(t)}\right]^2 \tag{8}$$

are the shape of the flowing layer and the simple shear rate in the flowing layer, respectively. Note that the expressions for the shape of the flowing layer differ in the two versions of the model; still, there are arguments that can lead to other shapes as well.[48]

Once again, upon introducing ϵ as the small parameter and nondimensionalizing the equations using the variables in Eq. (5), we can rewrite Eq. (7) as

$$v_x^B(x,y,t) = \frac{1}{\epsilon^2}\left[y + \epsilon\sqrt{L^2-x^2}\right], \tag{9a}$$

$$v_y^B(x,y,t) = \frac{xy}{\epsilon\sqrt{L^2-x^2}}. \tag{9b}$$

III. PARAMETER SPACE STUDY

The model described in Sec. II has one free parameter, namely, ϵ, which is typically fitted based on experimental observations,[29] and, once the geometry of the tumbler is fixed, the fill fraction ϕ can also be varied. This results in a two-dimensional parameter space for the dynamical system. Establishing the effect of the fill fraction on the mixing properties of a tumbler is of significant practical interest.[49]

Without loss of generality, since all polygonal tumblers share the same basic geometric features,[5] we use a square tumbler as the featured example in the present work. Also, all simulations shown are performed using model A from

Sec. II A (depth-averaged streamwise velocity is independent of position), since the Poincaré sections are qualitatively the same for all the various flowing layer shapes and velocity profiles.[5,36,50]

A. Overview of the dynamics

Figure 3 contains four progressions, each for a different fill fraction ϕ, of Poincaré sections showing the effects of diminishing ϵ.[51] This illustrates qualitatively how the structure of the flow changes as the flowing layer vanishes (from left to right) and the effect of increasing the fill fraction ϕ (from top to bottom). Although many transitions and bifurcations occur in the Poincaré section's pattern as ϵ and ϕ are varied, Fig. 3 illustrates the basic trends. As ϵ decreases, for $\phi<0.5$ the large island (i.e., elliptic periodic points surrounded by the KAM curves[3]) on the main diagonal of the tumbler are "pushed out" toward the corners and eventually disappear, giving way to several rings of island chains. Meanwhile, for $\phi>0.5$, the largely regular pattern present for $\epsilon=\mathcal{O}(1)$ breaks up as $\epsilon\to 0$, giving rise to a "chaotic sea" punctuated by islands whose locations coincide with symmetries of the tumbler.[5]

Furthermore, at $\epsilon\approx 10^{-1}$, for any given fill fraction, the Poincaré section has qualitatively reached a consistent pattern. That is, the location of the periodic points (specifically, the elliptic ones and the corresponding islands) does not change significantly for any $\epsilon\lesssim 10^{-1}$ at that fill fraction. In other words, the dynamics are not structurally different for any values of ϵ below this threshold, as $\epsilon\to 0$.

Naturally, there are differences in the Poincaré sections for different fill fractions ϕ. However, the most striking is that $\phi=0.5$ is an *exception*, in that the dynamics for $\phi=0.5$ and $\epsilon\to 0$ differ significantly from those for $\phi\neq 0.5$ and $\epsilon\to 0$. The chaotic region in the 50% full tumbler vanishes with the flowing layer. This also occurs in a 50% full elliptical tumbler, as shown in Fig. 7 of Khakhar *et al.*[29] While for all non-half-full tumblers a significant chaotic region remains for all $\epsilon\ll 1$, the corresponding one in the half-full tumbler diminishes with ϵ, and the elliptic regions dominate the limiting Poincaré section for finite ϵ. This observation led to the discovery of the streamline jumping mechanism,[20] upon which we elaborate below.

Based on the discussion of streamline crossing in Sec. II, the presence of a significant chaotic region in the Poincaré sections for $\phi\neq 0.5$ as $\epsilon\to 0$ is unexpected. This is because streamline crossing can only occur in the flowing layer of this tumbled granular flow. If the flowing vanishes, streamline crossing cannot occur. Yet, complicated (perhaps even chaotic in some sense yet to be made precise) dynamics persist due to streamline jumping.

Finally, note that this numerical exploration of the parameter space constitutes a qualitative perturbation analysis of the governing dynamical system. Figure 3 clearly shows that the $\epsilon=0$ dynamics form the *basic state* (i.e., the "skeleton") for the dynamics at any $\epsilon\ll 1$. Of course, this follows from perturbation theory, whereby one seeks solutions of the form $\Psi(x,y,t;\epsilon)=\Sigma_{i=0}^{\infty}\epsilon^i\Psi_i(x,y,t)$, because setting $\epsilon=0$ in the formal expansion yields the basic state $\Psi(x,y,t;0)\equiv\Psi_0(x,y,t)$. Then, for $0<\epsilon\ll 1$, $\Psi\approx\Psi_0$ to the leading order. The similarity between the seventh column (corresponding to Ψ_0) and the fifth and sixth columns [corresponding to $\Psi_0+\mathcal{O}(\epsilon)$] in Fig. 3 illustrates this reasoning. Although, as mentioned earlier, not all theorems carry over to the nonsmooth dynamics of tumbled granular flows, this observation shows clearly that the fundamental ideas do apply, and the limiting behavior is the template for the dynamics of nearby states in the parameter space.

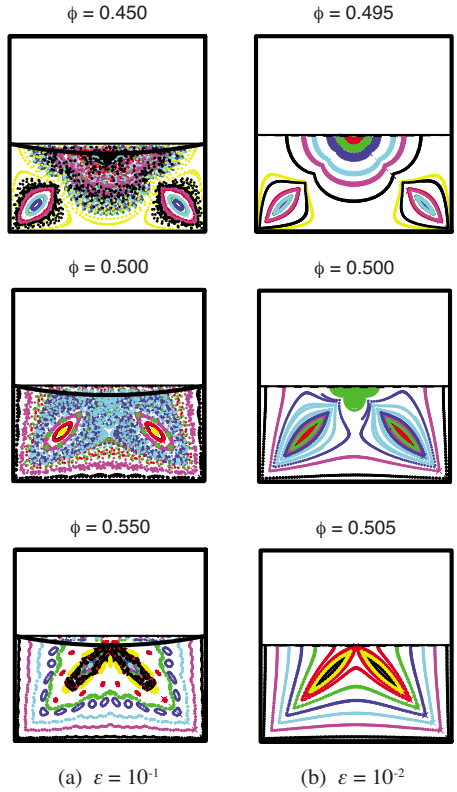

FIG. 4. (Color online) Two progressions of 500-period Poincaré sections near the exceptional fill fraction $\phi=0.5$, illustrating the concept of dynamic similarity of the patterns for two values of ϵ and the sensitive behavior of the $\phi=0.5$ state as $\epsilon\to 0$.

B. Sensitivity of the half-full state as $\epsilon\to 0$

From the qualitative perturbation analysis point of view, it is worthwhile to focus further on the exceptional case of $\phi=0.5$. In fact, the Poincaré section (as a function of ϕ) changes very quickly for fixed $\epsilon\ll 1$ and $\phi\approx 0.5$,[51] suggesting that in some sense this state is an "unstable equilibrium." Figure 4 depicts the behavior near $\phi=0.5$ for (a) $\epsilon=10^{-1}$ and (b) $\epsilon=10^{-2}$. Each column of the figure shows the transition of the Poincaré section pattern as ϕ is varied from a value slightly below to a value slightly above 0.5. Note that, for the two choices of ϵ, different ranges of ϕ are shown, chosen so that the left and right columns are *dynamically similar*. That is, the location of the elliptic periodic points (and the attendant islands) on the diagonals of the tumbler is approximately the same for the given pairs of the parameters ϕ and ϵ. It is immediately evident that as the flowing layer thickness decreases, the range of ϕ for dynamic similarity decreases.

The sensitive behavior near $\phi=0.5$ has been observed previously;[11] however, we are now able to explain its origin. Based on the notion of dynamic similarity, we can conclude that as $\epsilon\to 0$ similar patterns occur at values of ϕ increasingly closer to 0.5, eventually "collapsing" onto the $\phi=0.5$ state. That is, for $\epsilon=0$, the square tumbler does not possess a Poincaré section whose prominent feature is two large elliptic islands on its diagonal, for any ϕ near 0.5. This behavior clearly illustrates the singular perturbation nature of the $\epsilon\to 0$ limit; a "solution" (or Poincaré section pattern in our qualitative perturbation analysis language) is lost as the small parameter goes to zero.

IV. THE VANISHING FLOWING LAYER LIMIT

The limit $\epsilon\to 0$ is singular, and it is a particularly difficult one to study analytically because the dynamical system is nonsmooth. Fortunately, due to the geometrically constrained nature of tumbled flows, it is possible to derive the governing limiting dynamical system as the flowing layer vanishes.

A. An infinitely thin, infinitely strong flowing layer

The most basic consequence of letting $\epsilon\to 0$ is that $\delta_0 \equiv \epsilon L\to 0$ also, since L is finite for all t. Thus, under both versions of the continuum model presented in Sec. II, the flowing layer becomes an infinitely thin *interface* as ϵ vanishes, collapsing onto the free surface of the granular matter in the container.

To understand the dynamics of the infinitely thin flowing layer, we can evaluate the surface velocity (i.e., the velocity at the free surface) from Eqs. (6) and (9),

$$v_x^A(x,0,t)=\frac{L}{\epsilon},\quad v_y^A(x,0,t)=0, \tag{10a}$$

$$v_x^B(x,0,t)=\frac{1}{\epsilon}\sqrt{L^2-x^2},\quad v_y^B(x,0,t)=0, \tag{10b}$$

where Eq. (10a) is under the assumption of a depth-averaged streamwise velocity independent of the position within the flowing layer, and Eq. (10b) is under the assumption of a constant simple shear rate within the flowing layer. Note that $v_y^A(x,0,t)=v_y^B(x,0,t)=0$ must always be the case because the free surface of the flow is a "rigid lid" (no particles can leave or enter through it).

Now, we can define the average *speed* of a particle over the length of the free surface over a period of the flow as

$$\bar{V}_{\text{surf}}=\frac{1}{T_f}\int_0^{T_f}\frac{1}{2L}\int_{-L}^{+L}\sqrt{v_x^2+v_y^2}\big|_{y=0}\,\mathrm{d}x\mathrm{d}t, \tag{11}$$

which can be combined with the results in Eq. (10) to yield

$$\bar{V}_{\text{surf}}^A=\frac{\bar{L}}{\epsilon},\quad \bar{V}_{\text{surf}}^B=\frac{\pi\bar{L}}{4\epsilon}, \tag{12}$$

where $\bar{L}=1/T_f\int_0^{T_f}L(t)\mathrm{d}t$ and $T_f=2\pi/n$ is the (dimensionless) flow period as defined in the Appendix. The second result generalizes that for a circular tumbler presented by Sturman *et al.*[21] Taking the limit $\epsilon\to 0$, both $\bar{V}_{\text{surf}}^A,\ \bar{V}_{\text{surf}}^B\to\infty$. Therefore, the particle velocities in the vanishingly thin flowing layer become infinite.

Turning to the mechanics of the infinitely thin flowing layer, we can evaluate the shear rate at the free surface,

$$\dot{\gamma}_{\text{surf}}(x,t):=\dot{\gamma}_{yx}(x,0,t)=\left(\frac{\partial v_y}{\partial x}+\frac{\partial v_x}{\partial y}\right)\Big|_{y=0}. \tag{13}$$

Then, from Eqs. (6) and (9), respectively, we have

$$\dot{\gamma}_{\text{surf}}^A(x,t)=\frac{1}{\epsilon^2}\left(\frac{L^2}{L^2-x^2}\right),\quad \dot{\gamma}_{\text{surf}}^B(x,t)=\frac{1}{\epsilon^2}. \tag{14}$$

Of course, $\dot{\gamma}_{\text{surf}}^B=\text{const}$ as required by the assumption under which this model is derived. Letting $\epsilon\to 0$, we have $\dot{\gamma}_{\text{surf}}^A\to\infty$, since $L^2/(L^2-x^2)$ is bounded away from zero for all $x\in[-L,L]$ and all $t\geq 0$; similarly, $\dot{\gamma}_{\text{surf}}^B\to\infty$ as $\epsilon\to 0$. This means that the shear rate in the flowing layer becomes unbounded as its thickness vanishes, which is why we referred to the vanishing shear layer as "infinitely strong" in the Sec. IV A heading. As was the case with the mean surface speed, both continuum models introduced in Sec. II give the same result. Therefore, the limiting ($\epsilon\to 0$) governing dynamical system is *identical* for *both* versions of the continuum model.

To an extent, the result that the surface velocity and shear rate are infinite in the infinitely thin flowing layer limit seems obvious. Nevertheless, it is important to establish this directly from the continuum model(s) of the flow.

At this point, one detail remains, namely, how do particles traverse a region with infinite shear rate? To elucidate this, consider a circular tumbler. Under both versions of the continuum model, the flowing layer shape δ is symmetric about $x=0$. In this geometry, the horizontal displacement of the free surface midpoint, i.e., $g(t)$, is identically zero, so the flowing layer is also symmetric about $\tilde{x}=0$. This combined with the fact that $\delta_0=\text{const}$ (since $L=\text{const}$) means that the streamlines in the flowing layer are symmetric about $\tilde{x}=x=0$. Consequently, if a particle reaches the infinitely thin flowing layer ($y=0$) at the horizontal location $x_{\text{enter}}(<0)$ at time $t=t_{\text{enter}}$, then it leaves the flowing layer at $x_{\text{exit}}=-x_{\text{enter}}$ (equivalently, $\tilde{x}_{\text{exit}}=-\tilde{x}_{\text{enter}}$) at some later time.

In a noncircular tumbler, $\delta_0=\delta_0(t)$ for finite ϵ but $\lim_{\epsilon\to 0}\delta_0(t)=0$, so δ_0 becomes constant in the limit. This combined with the fact that particles traverse the infinitely thin flowing layer *instantaneously* ($V_{\text{surf}}=\infty$), so they do not "feel" the change in $g(t)$ with time, means that particles must, as in the circular tumbler, leave the flowing at the streamwise location x_{exit} (on the interface) corresponding to the reflection of the position x_{enter} they entered across the free surface midpoint, i.e., $x_{\text{exit}}=-x_{\text{enter}}$, which justifies the *assumption* made in the literature.[19] Using the rigid coordinate system with origin at C, $\tilde{x}_{\text{exit}}=-\tilde{x}_{\text{enter}}+2g(t_{\text{enter}})$ is the new location of the particle; clearly, if $g(t_{\text{enter}})\neq 0$ then the particle will not remain on the same streamline after crossing the flowing layer.

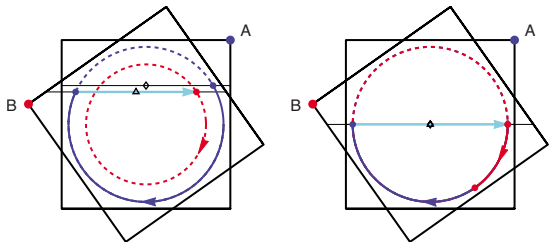

FIG. 5. (Color online) Illustration of how streamline jumping occurs in two tumblers with infinitely thin flowing layers ($\epsilon=0$) but with different fill fractions. Note the absence of a streamline jumping mechanism in (b). In both, the rotation is clockwise.

B. How streamline jumping leads to physical mixing in the absence of a flowing layer

As we have just established, in a noncircular tumbler, the time-dependent horizontal motion of the midpoint of the flowing layer O allows particles to "jump" from one solid-body-rotation streamline to a *different* one. This streamline jumping mechanism[20] is illustrated in Fig. 5. For a 73% full tumbler, in Fig. 5(a), a particle initially, i.e., at $t=0$ when the tumbler is in orientation A, on the solid blue streamline jumps onto the dashed red streamline upon reaching the flowing layer (illustrated by the light blue arrow) at some time $t>0$ when the tumbler is in orientation B. The location of the flowing layer's midpoint in tumbler orientation A is denoted by a small diamond, while that for tumbler orientation B is denoted by a small triangle; they do not coincide for $\phi=0.73$. In Fig. 5(b), where the case of a 50% full square tumbler is illustrated, the midpoint of the flowing layer remains coincident with the center of rotation of the tumbler for all times, i.e., the horizontal and vertical displacements of the moving coordinate system $g(t)=h(t)\equiv 0\ \forall t$. Clearly, no streamline jumping is possible, and particles are always transferred to the same solid-body-rotation streamline. Therefore, the precise mechanism leading to complex dynamics in a granular tumbled flow with no shear layer is streamline jumping, not simply time periodic disturbances due to the shape of the container leading to chaos in the flow, which has been suggested previously.[19]

Now, it is clear from Fig. 5(b) why the Poincaré section of a tumbled granular flow in a 50% full square tumbler with $\epsilon=0$ shown in Fig. 3(g) should consist only of dots on the lower halves of the main diagonals of the square. This is because all the tracer particles that are initially seeded on the diagonal (see Appendix) remain on closed circular streamlines for all time. Thus, the stroboscopic map captures them twice at their initial location and twice at the mirror-image location on the opposite diagonal for each full rotation of the tumbler (four flow periods for a square tumbler). This geometric reasoning is valid for *any* convex noncircular tumbler, not just the square one used to illustrate the concept in Fig. 5. The fundamental result is that the *necessary* (but certainly not sufficient) condition for complicated particle trajectories in a tumbled granular flow with a vanishing flowing layer is that, at the given fill fraction ϕ, the displacements g and h vary with time.

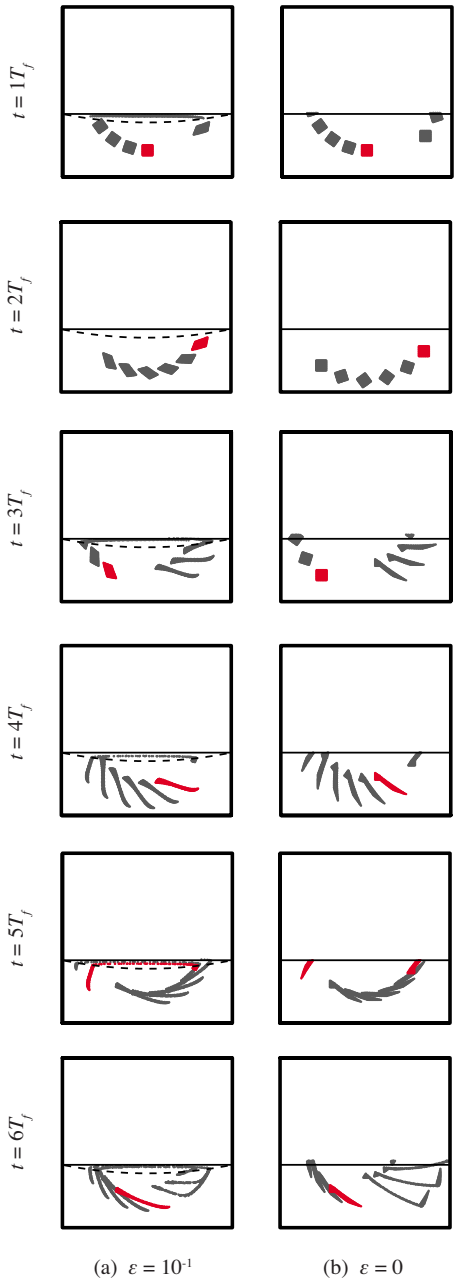

FIG. 6. (Color online) Spread of a square blob of tracer particles in a square tumbler over six flow periods for both a finite and a vanishingly thin flowing layer. The tumbler rotates clockwise.

To better understand how streamline jumping leads to *physical* mixing of matter in the tumbler, we present a "blob deformation" computational experiment in Fig. 6. In each column, the evolution of a square "blob" of tracer particles over six consecutive flow periods T_f is illustrated. In each plot, the initial [i.e., at $t=(p-1)T_f$, where $p\in\{1,2,3,4,5,6\}$] shape and location of the blob are shown in red; subsequently, the location and shape are plotted at intervals of $0.2T_f$ up to $t=pT_f$; the superimposed orientation of the container also corresponds to $t=pT_f$. The simulation is performed for both (a) a finite flowing layer ($\epsilon=10^{-1}$) and (b) an infinitely thin one ($\epsilon=0$).

Clearly, the evolution of the "blobs" in Figs. 6(a) and 6(b) is similar. As discussed in Sec. III A, this is expected

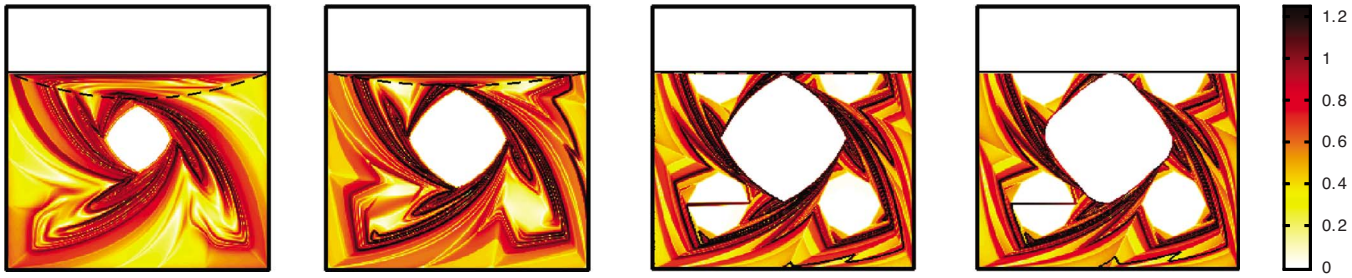

(a) $\varepsilon = 2\text{x}10^{-1}$ (b) $\varepsilon = 10^{-1}$ (c) $\varepsilon = 10^{-2}$ (d) $\varepsilon = 0$

FIG. 7. (Color online) FTLE field $\sigma(X,Y;t_0=0,\tau=-14T_f)$ in a 75% full square tumbler for four different values of ϵ, revealing the manifold structure of the flow and how it is affected by the flowing layer's thickness.

since the $\epsilon=0$ dynamics are the template for the dynamics with $\epsilon \ll 1$. This illustrates, even more conclusively than the Poincaré sections in Fig. 3, that the underlying geometric effects that make streamline jumping possible are very significant in realistic parameter regimes (e.g., $\epsilon=10^{-1}$, a value easily achieved experimentally).

To elucidate this further, imagine a line segment of tracer points ("particles") reaching the infinitely thin flowing layer parallel to it. The entire line segment is reflected across O instantaneously, and its length remains unchanged; this appears to occur for $t \in [0, T_f]$ in the first row of Fig. 6(b). However, this is *not* the typical case. If the segment enters the flowing layer at an angle, each point on it reflects across O at a slightly different time and tumbler orientation. This shifts the points on the segment to nearby streamlines, eventually *spreading* them further apart than they were initially, which results in mixing; this is very clearly seen to occur for $t \in [2T_f, 3T_f]$ in the third row of Fig. 6(b).[52] Similarly, this kind of spreading of nearby points, due entirely to the horizontal motion of the flowing layer's midpoint O, persists in the case of a finite-thickness flowing layer [Fig. 6(a)], although the stretching due to shear within it spreads the points even further apart as the last two rows show.

It is important to note that this mechanism of mixing is unrelated to diffusion (i.e., particle dispersal through random collisions) and works despite the absence of a flowing layer and streamline crossing; it is purely geometric. Of course, in experiments, diffusion due to the finite size of particle cannot be eliminated but its effect on mixing is weak compared with that of advection.[29] Moreover, this new geometric insight into the physics of granular mixing represents a fundamental departure from the "traditional" way of thinking about chaotic advection and brings with it new mathematical insights, which we discuss in Sec. V.

C. Finite-time Lyapunov exponents and manifold structure

A more quantitative way to identify the geometric effects that lead to mixing in the absence of a flowing layer is through the (largest) FTLE field of the flow, which is defined as[14,15]

$$\sigma(X,Y;t_0,\tau) = \frac{1}{|\tau|}\ln\sqrt{\Lambda_{\max}(\mathbf{C}(X,Y;t_0,\tau))}, \tag{15}$$

where $(X,Y)^\top$ are the coordinates in the initial (i.e., reference) configuration of the tumbler at $t=t_0$, $\mathbf{C}(X,Y;t_0,\tau)$ is the (right) Cauchy–Green deformation tensor[3] at time $t=t_0+\tau$ with respect to time $t=t_0$, $\Lambda_{\max}(\cdot)$ represents the maximum eigenvalue (in absolute value) of its argument, and τ is a free parameter that can be either positive or negative. Taking the limit $\tau\to\infty$, assuming the flow satisfies the requisite conditions, Eq. (15) becomes the usual definition of an infinite-time Lyapunov exponent.[2,15] This measure of the local "stretching" of the underlying continuum by the flow is related to a well-known quantity in fluid mixing, namely, the *length stretch*[3,4] $\lambda \equiv (\mathbf{C}:\mathbf{MM})^{1/2}$ of a material filament with initial orientation $\mathbf{M}$. From the Rayleigh–Ritz theorem, which states that $\max_{\|\mathbf{M}\|=1}\mathbf{C}:\mathbf{MM}=\Lambda_{\max}(\mathbf{C})$, it is clear that $\sqrt{\Lambda_{\max}(\mathbf{C})}$ is precisely the *maximal* local length stretch. Also, note that $\mathbf{C}$ is a positive definite tensor so that $\sqrt{\Lambda_{\max}(\mathbf{C})}$ is always real and nonzero.

Figure 7 shows how the FTLE field σ varies with ϵ in a 75% full square tumbler.[53] First, it is important to note that a LCS is defined as a *ridge* of σ, i.e., a curve across which the normal gradient $\hat{\boldsymbol{n}}\cdot\nabla\sigma$ has a local maximum.[15] Without dwelling on the technical details of this definition, it suffices to qualitatively identify the ridges with the darkest areas in the plots in Fig. 7. The importance of the ridges is that the mass flux across them is negligible.[15] In addition, they are analogs (in flows with arbitrary time dependence) to the stable (if $\tau>0$) or the unstable (if $\tau<0$) manifolds of time-independent (or time-periodic) flows.[12–15] Indeed, it is immediately clear that Fig. 7(b) is almost identical to Fig. 12 of Meier *et al.*,[6] where the unstable manifold of the hyperbolic periodic points of the tumbled granular flow in a 75% full square is traced out.

Likewise, the elliptic periodic points and their corresponding KAM curves, which can be seen on the lower diagonals of the tumbler in the bottom row of Fig. 3, appear as large bright regions (i.e., low σ) in the FTLE fields shown in Fig. 7. Figure 7 complements Fig. 3 in that the former clearly illustrates the effects of the hyperbolic periodic points (manifolds), while the latter clearly illustrates the effects of the elliptic periodic points (KAM islands). The hyperbolic peri-

odic points are more difficult to locate visually, but numerical calculations[6] have shown that they are located on the outer ridges to the left, right, and below the main unmixed core in the tumbler. Two of them are roughly on the horizontal centerline of the tumbler, while the third is slightly below the horizontal line connecting the elliptic points on the lower diagonals of the tumbler.

Note that the thin horizontal line of large σ through the lower-left unmixed core in Fig. 7 is not part of the manifold but merely an artifact of the FTLE calculation. At the moment the flow is "frozen" (i.e., at $t=t_0+\tau$ for any given τ) and the FLTE field computed, there is a slice (its thickness proportional to that of the flowing layer) of material points of the continuum that were initially close to each other but are now on opposite ends of the flowing layer, leading to an artificially high value of σ for these points. Of course, if τ is chosen slightly larger, these points will once again be on the same side of the flowing layer, but there will be a different slice of points that become separated.

Figure 7 reveals (quantitatively) two features of the $\epsilon \to 0$ limit of quasi-two-dimensional granular tumbled flows. First, the FTLEs of material points in the continuum (with the exception of the regions of unmixed material typical for this tumbler geometry and fill fraction) are largely independent of ϵ, and therefore independent of the shear in the flowing layer. Thus, mixing is dominated by the underlying geometric effects that cause streamline jumping. Second, the manifold structure of the flow for $\epsilon=0$ is the template for the manifold structure of flows with $\epsilon \ll 1$. This corroborates the conclusions drawn from the Poincaré section study in Sec. III A.

V. THE LIMITING DYNAMICS AS A PIECEWISE ISOMETRY

In Sec. IV, it was shown that when $\epsilon=0$ particles in the tumbled granular flow undergo solid body rotation until they reach the flowing layer interface and jump across it. In the most general sense, this kind of dynamical system is termed an *impacting hybrid system*,[40] hybrid because of the coexistence of discrete (streamline jumping) and continuous (rotation) movements, impacting because of the discontinuous nature of the discrete movement. Furthermore, solid body rotation is just one example of a distance-preserving mapping or isometry.

Therefore, according to the definition of Deane,[24] the limiting ($\epsilon=0$) dynamical system is, specifically, a piecewise isometry (PWI)—a type of discontinuous dynamical system studied in detail only recently.[23] A number of results have been established showing that PWIs can exhibit the usual behaviors of nonlinear dynamical systems, namely, periodic points, quasiperiodicity, fractal structure, global attractors, and generally complex dynamics.[21,23,24,54,55]

To make the connection clearer, we construct the PWI explicitly in the spirit of previous efforts[19,28] to write the tumbled flow as a discrete-time map. First, we define the domain and range of the map in the coordinate system with origin at C (Fig. 1),

$$\mathcal{D}(t)=\{(\tilde{x},\tilde{y})^{\top} | \tilde{y}=h(t),\ \ 0<\tilde{x}-g(t)<L(t)\}, \tag{16a}$$

$$\mathcal{R}(t)=\{(\tilde{x},\tilde{y})^{\top} | \tilde{y}=h(t),\ \ -L(t)<\tilde{x}-g(t)<0\}, \tag{16b}$$

these are simply the left and right halves, respectively, of the flowing layer interface at time t. Then, the PWI takes the form of an affine transformation $\mathbf{\Omega}(t_1,t_2):\mathcal{D}(t_1)\to\mathcal{R}(t_2)$ that can be represented as

$$\mathbf{\Omega}(t_1,t_2)=\mathbf{T}(t_2)\circ\mathbf{R}\circ\mathbf{Q}(t_1,t_2), \tag{17}$$

where $\mathbf{Q}(t_1,t_2)$ is a rigid rotation from the initial position of the particle on the flowing layer at $t=t_1$ to its final position upon reaching the flowing layer again at $t=t_2$ (to be determined), $\mathbf{R}$ is a reflection about the $\tilde{y}$-axis, and $\mathbf{T}(t_2)$ is a shift along the $\tilde{x}$-axis at $t=t_2$. Each individual map of the PWI can be easily computed, and the composition of them is

$$\mathbf{\Omega}(t_1,t_2)=\begin{pmatrix} -\cos(\omega_z\bar{t}) & -\sin(\omega_z\bar{t}) & 2g(t_2) \\ -\sin(\omega_z\bar{t}) & \cos(\omega_z\bar{t}) & 0 \\ 0 & 0 & 1 \end{pmatrix}. \tag{18}$$

Here, $\bar{t}$ is the first positive solution of $h(t_1+\bar{t})=r_0\sin(\theta_0-\omega_z\bar{t})$, where $r_0=(\tilde{x}_1^2+\tilde{y}_1^2)^{1/2}$, $\theta_0=\tan^{-1}(\tilde{y}_1/\tilde{x}_1)$, and $(\tilde{x}_1,\tilde{y}_1)^{\top}\in\mathcal{D}(t_1)$ is a given starting position; clearly, $t_2=t_1+\bar{t}$. Note that $\mathbf{\Omega}$ must be applied to the homogeneous coordinates $(\tilde{x},\tilde{y},1)^{\top}$ and, in the present work, rotation is always clockwise with $\omega_z>0$. It is possible that no solution $\bar{t}$ exists, e.g., when a trajectory never reaches the flowing layer because it remains in the central unmixed core. Then, we can set $\bar{t}=\infty$.

Qualitatively speaking, Eq. (17) can be understood in terms of cutting and shuffling dynamics[21,22] as follows: $\mathbf{Q}$ "shuffles" by mapping each initial position on the flowing layer interface to a new location on the flowing later at a later time (and location in space), while $\mathbf{R}\circ\mathbf{T}$ "cuts" by reflecting and translating points along the flowing layer.

An important point here is that this map depends on the initial position of the trajectory; that is, for each $(\tilde{x}_1,\tilde{y}_1)^{\top}\in\mathcal{D}(t_1)$ the value of t_2 is different. Thus the image of *all* points in $\mathcal{D}(t_1)$ under the action of $\mathbf{\Omega}$ is quite complicated. In some sense, it is appropriate to call this a *nonlinear* PWI because map depends on the spatial coordinates implicitly through the need to determine when a given trajectory intersects the (moving) flowing layer again, unlike the PWIs found in the literature.[21–24]

An analysis of the PWI (18) goes beyond the scope of the present work, but a few comments can be made *a priori*. First, a crucial difference exists between a (discontinuous) PWI exhibiting complex behavior and a (continuous) dynamical system exhibiting chaotic behavior: in the case of the former there are no positive (infinite-time) Lyapunov exponents.[54] The latter is characterized precisely by its positive Lyapunov exponents. Second, under certain conditions, PWIs have been shown to have zero topological entropy,[56] while continuous chaotic dynamical systems have a positive one. This shows that typical PWIs do not possess the stretching characteristics that are universal for (continuous) chaotic dynamics[2] and fluid flows.[3,57] Indeed, it is easy to verify that all of the eigenvalues of the map $\mathbf{\Omega}$ have unit magnitude. Therefore, since the "basic state" of tumbled granular flows

is a PWI, as we have shown, granular mixing is fundamentally and mathematically very different from fluid mixing.

The questions of to what extent and in what sense can the complex dynamics resulting from the PWI discussed here be called "chaotic" remains open. For example, it was recently shown[55] that certain PWIs exhibit chaotic dynamics in the sense of Devaney: that is, the dynamical system exhibits (i) sensitive dependence on the initial conditions and (ii) is topologically transitive.[58] Although this result represents mathematical progress, the most important questions regarding physical mixing are those relating to the ergodic theory of PWIs.

VI. CONCLUSION

In the present work, we studied a class of flows of granular matter in quasi-two-dimensional rotating tumblers through numerical simulation and the qualitative theory of dynamical systems. Although the governing Eq. (1) is quite difficult (if not intractable) to study analytically, we were able to successfully extract the dynamics using tools such as the Poincaré section and FTLEs. In addition, we established that a small parameter (namely, the ratio of the flowing layer's maximal depth to half its length) and the fill fraction of the container define a two-dimensional phase space where the dynamics occur. An important result is that the fill fraction has a significant effect on the limiting (i.e., no-shear-layer) dynamics, with the 50% fill level being an exceptional case in even-sided polygonal tumblers (and, in general, tumblers for which there exists a ϕ such that the horizontal distance between the flowing layer's midpoint and the center of rotation remains unchanged for all time). This exceptional case also illustrates the singular perturbation nature of the limit as the chosen small parameter tends to zero.

The main result is that as the flowing layer vanishes and streamline crossing (the hallmark of chaotic mixing) becomes impossible, complex dynamics persist due to streamline jumping. This is, as far as we know, a new mechanism leading to complex dynamics in this type of nonsmooth dynamical system. Without parallel in the mixing of fluids, where linked twist maps describe the geometry of mixing, streamline jumping shows that the underlying geometric description of granular flows is in the form of a PWI. Indeed, PWIs were also found to play an important role in three-dimensional spherical tumblers.[21,22] Although, previously, PWIs were only applied in signal processing,[24] it is clear now that they also provide the framework for granular mixing. In addition, this cutting and shuffling mechanism of granular mixing may be present in geophysical thrust systems[59] and periodically reoriented potential flows.[60,61]

Much remains to be done, however, with regard to the applicability to mixing in granular tumbled flows of previous theoretical results on (infinite-time) Lyapunov exponents[54] and topological entropy.[56] Mathematical mixing also deserves attention as the ergodic properties of PWIs have yet to be studied in detail. Also, the analysis of various errors in the computation of mixing in chaotic systems[62] should be extended to the nonsmooth dynamical systems presented here. In addition, it is also important to reproduce the present theoretical and computational results in the laboratory. Preliminary experimental results show that the kinematics of monodisperse tumbled granular mixtures are essentially determined by the $\epsilon=0$ case studied herein. The effects of a diminishing flowing layer on the segregation patterns of tumbled bidisperse granular mixtures also require further study—the question of whether a thinner flowing layer leads to more or less segregation in the mixture is of practical significance.

ACKNOWLEDGMENTS

We thank Stephen Wiggins, Rob Sturman, and Michał Branicki for valuable input and fruitful discussions on PWIs. The careful reading and insightful comments by the reviewers are also much appreciated. I.C.C. was supported by a Walter P. Murphy Fellowship from the Robert R. McCormick School of Engineering and Applied Science at Northwestern University.

APPENDIX: NUMERICAL IMPLEMENTATION DETAILS

Following Cisar *et al.*,[5] to solve the governing equations numerically we convert them to the rigid coordinate system with origin at the center of rotation of the tumbler C, which is also the geometric centroid of the container in the present work. Then, the appropriate coordinate transformation is $x \to \tilde{x} - g(t)$, $y \to \tilde{y} - h(t)$, where $g(t)$ and $h(t)$ are the horizontal and vertical (signed) distances, respectively, between the center of rotation of the tumbler C and the midpoint of the free surface O (see Fig. 1). In the rigid coordinate system, the vertical and horizontal directions are defined with respect to the initial configuration of the tumbler, which we choose to be such that one side is horizontal.

We employ the time-stepping (as opposed to event-driven) approach[40] to the numerical simulation of nonsmooth dynamical systems. The classical fourth-order Runge–Kutta time-integration scheme is used for the equations in the flowing layer, while the symplectic Euler[63] scheme is used to integrate the equations of solid-body rotation. A time step $\Delta t = 5 \times 10^{-5} T_f$ is taken, where $T_f = T/n$ is flow period for an n-sided tumbler, and $T = 2\pi/\omega_z$ is the period of rotation. In terms of the dimensionless variables introduced in Eq. (5), $T = 2\pi$ and $T_f = 2\pi/n$. For simulations with $\epsilon \leq 10^{-3}$, the time step was reduced to $\Delta t = 10^{-6} T_f$ for numerical stability.

In all Poincaré sections shown, 13 tracer particles [uniformly distributed along the line connecting the point $(0, \min\{h(0), 0\})$ to the lower-right corner of the tumbler] are advected in this manner for 500 periods. The angular speed of the tumbler is always $\omega_z = 2\pi$ in the clockwise (i.e., "negative" mathematical) direction. Finally, the tumbler "radius" is taken equal to 1 or, equivalently, the side length is $S = \sqrt{2}$.

In computing the FTLE field of the flow, the granular continuum in the initial configuration, taken to be at time $t = t_0 = 0$ for all cases presented here, is discretized into 210×210 uniformly distributed points throughout the filled area of the tumbler. These are advected with flow, for the length of time τ, as described above for the Poincaré sections. At the final time $t = t_0 + \tau \equiv \tau$, the deformation gradient $\mathbf{F} = \partial \boldsymbol{x} / \partial \boldsymbol{X}$ (where $\boldsymbol{x}$ and $\boldsymbol{X}$ are the coordinates in the deformed and reference configurations, respectively) is com-

puted by a central finite difference approximation,[6,15] whence the (right) Cauchy–Green deformation tensor is simply $\mathbf{C}=\mathbf{F}^{\top}\mathbf{F}$.

[1]S. H. Strogatz, *Nonlinear Dynamics and Chaos* (Westview, Cambridge, 2001).
[2]S. Wiggins, *Introduction to Applied Nonlinear Dynamical Systems and Chaos*, 2nd ed. (Springer-Verlag, Berlin, 2003).
[3]J. M. Ottino, *The Kinematics of Mixing: Stretching, Chaos, and Transport* (Cambridge University Press, Cambridge, 1989).
[4]J. M. Ottino, Annu. Rev. Fluid Mech. **22**, 207 (1990).
[5]S. E. Cisar, P. B. Umbanhowar, and J. M. Ottino, Phys. Rev. E **74**, 051305 (2006).
[6]S. W. Meier, S. E. Cisar, R. M. Lueptow, and J. M. Ottino, Phys. Rev. E **74**, 031310 (2006).
[7]P. Porion, N. Sommier, A.-M. Faugère, and P. Evesque, Powder Technol. **141**, 55 (2004).
[8]J. S. Brooks and J. A. Cothern, Physica B **294–295**, 721 (2001).
[9]J.-O. Aidanpää, H. H. Shen, R. B. Gupta, and M. Babić, Mech. Mater. **16**, 153 (1993).
[10]A. Alexeev, A. Goldshtein, and M. Shapiro, Powder Technol. **123**, 83 (2002).
[11]K. M. Hill, D. V. Khakhar, J. F. Gilchrist, J. J. McCarthy, and J. M. Ottino, Proc. Natl. Acad. Sci. U.S.A. **96**, 11701 (1999).
[12]S. Wiggins, Annu. Rev. Fluid Mech. **37**, 295 (2005).
[13]M. Branicki and S. Wiggins, Nonlinear Processes Geophys. **17**, 1 (2010), e-print arXiv:0908.1129
[14]G. Haller, Physica D **149**, 248 (2001).
[15]S. C. Shadden, F. Lekien, and J. E. Marsden, Physica D **212**, 271 (2005).
[16]M. Mathur, G. Haller, T. Peacock, J. E. Ruppert-Felsot, and H. L. Swinney, Phys. Rev. Lett. **98**, 144502 (2007).
[17]J. Rajchenbach, Phys. Rev. Lett. **65**, 2221 (1990).
[18]G. H. Ristow, *Pattern Formation in Granular Materials* (Springer-Verlag, Berlin, 2000).
[19]T. Elperin and A. Vikhansky, Chaos **9**, 910 (1999).
[20]I. C. Christov, J. M. Ottino, and R. M. Lueptow, Phys. Rev. E **81**, 046307 (2010).
[21]R. Sturman, S. W. Meier, J. M. Ottino, and S. Wiggins, J. Fluid Mech. **602**, 129 (2008).
[22]G. Juarez, "Mixing and segregation dynamics of granular mixtures in rotating tumblers," Ph.D. thesis, Northwestern University, 2009.
[23]A. Goetz, in *Fractals in Graz 2001*, edited by P. Grabner and W. Woess (Birkhäuser, Basel, 2002), pp. 135–144.
[24]J. H. B. Deane, Meccanica **41**, 241 (2006).
[25]R. Sturman, J. M. Ottino, and S. Wiggins, *The Mathematical Foundations of Mixing* (Cambridge University Press, Cambridge, 2006).
[26]I. S. Aranson and L. S. Tsimring, Phys. Rev. Lett. **82**, 4643 (1999).
[27]I. S. Aranson, L. S. Tsimring, and V. M. Vinokur, Phys. Rev. E **60**, 1975 (1999).
[28]D. V. Khakhar, J. J. McCarthy, T. Shinbrot, and J. M. Ottino, Phys. Fluids **9**, 31 (1997).
[29]D. V. Khakhar, J. J. McCarthy, J. F. Gilchrist, and J. M. Ottino, Chaos **9**, 195 (1999).
[30]T. Elperin and A. Vikhansky, Phys. Rev. E **62**, 4446 (2000).
[31]T. Elperin and A. Vikhansky, Physica A **303**, 48 (2002).
[32]K. Hutter and K. R. Rajagopal, Continuum Mech. Thermodyn. **6**, 81 (1994).
[33]K. K. Rao and P. R. Nott, *An Introduction to Granular Flow* (Cambridge University Press, Cambridge, 2008).
[34]J. M. N. T. Gray, J. Fluid Mech. **441**, 1 (2001).
[35]S. P. Pudasaini and K. Hutter, *Avalanche Dynamics* (Springer-Verlag, Berlin, 2007).
[36]S. W. Meier, R. M. Lueptow, and J. M. Ottino, Adv. Phys. **56**, 757 (2007).
[37]I. S. Aranson and L. S. Tsimring, *Granular Patterns* (Oxford University Press, New York, 2009).
[38]H. Aref, Philos. Trans. R. Soc. London, Ser. A **333**, 273 (1990).
[39]M. Kunze, *Non-Smooth Dynamical Systems* (Springer-Verlag, Berlin, 2000).
[40]M. di Bernardo, C. J. Budd, A. R. Champneys, and P. Kowalczyk, *Piecewise-Smooth Dynamical Systems* (Springer-Verlag, Berlin, 2008).
[41]N. Jain, J. M. Ottino, and R. M. Lueptow, Phys. Fluids **14**, 572 (2002).
[42]N. Jain, J. M. Ottino, and R. M. Lueptow, J. Fluid Mech. **508**, 23 (2004).
[43]G. D. R. MiDi, Eur. Phys. J. E **14**, 341 (2004).
[44]I. S. Aranson, L. S. Tsimring, F. Malloggi, and E. Clément, Phys. Rev. E **78**, 031303 (2008).
[45]S. J. Fiedor and J. M. Ottino, J. Fluid Mech. **533**, 223 (2005).
[46]R. Sturman and S. Wiggins, New J. Phys. **11**, 075031 (2009).
[47]H. A. Makse, Phys. Rev. Lett. **83**, 3186 (1999).
[48]T. Elperin and A. Vikhansky, Europhys. Lett. **42**, 619 (1998).
[49]H. M. Jaeger, S. R. Nagel, and R. P. Behringer, Rev. Mod. Phys. **68**, 1259 (1996).
[50]S. E. Cisar, "Development and application of discrete and continuum models of kinematics and dynamics of granular flow," Ph.D. thesis, Northwestern University, 2006.
[51]See supplementary material at http://dx.doi.org/10.1063/1.3368695 for movies illustrating the transitions in the Poincaré section pattern for the 37% and 50% full tumblers with ϵ ranging from 3×10^{-1} to 10^{-2} (step of -5×10^{-3}) and movies illustrating the effect of ϕ, ranging from 0.35 to 0.75 (step of 0.005), on the Poincaré section pattern for square tumblers with $\epsilon=10^{-1}$ and $\epsilon=10^{-2}$.
[52]Note that, when discussing the effects of streamline jumping on the blob of particles, we have strictly used the term "spreading" instead of "stretching" because this geometric effect is not due to either extensional or shear strain, which is typically how stretching is defined in continuum mechanics.
[53]Due to the discontinuous nature of the flow for $\epsilon=0$, Eq. (15) no longer defines a FTLE in a rigorous mathematical way. Nevertheless, we choose to use the term even in this case because the *analogy* between Fig. 7(d) and the FTLE field is clear.
[54]X.-C. Fu and J. Duan, Physica D **237**, 3369 (2008).
[55]B. Kahng, Chaos **19**, 023115 (2009).
[56]J. Buzzi, Ergod. Theory Dyn. Syst. **21**, 1371 (2001).
[57]G. A. Voth, G. Haller, and J. P. Gollub, Phys. Rev. Lett. **88**, 254501 (2002).
[58]R. L. Devaney, *An Introduction to Chaotic Dynamical Systems*, 2nd ed. (Westview, Cambridge, 2003).
[59]S. E. Boyer and D. Elliott, AAPG Bull. **66**, 1196 (1982).
[60]D. R. Lester, G. Metcalfe, M. G. Trefry, A. Ord, B. Hobbs, and M. Rudman, Phys. Rev. E **80**, 036208 (2009).
[61]G. Metcalfe, D. Lester, A. Ord, P. Kulkarni, M. Trefry, B. E. Hobbs, K. Regenaur-Lieb, and J. Morris, Philos. Trans. R. Soc. London, Ser. A **368**, 217 (2010).
[62]A. Soulvaiotis, S. C. Jana, and J. M. Ottino, AIChE J. **41**, 1605 (1995).
[63]B. Leimkuhler and S. Reich, *Simulating Hamiltonian Dynamics* (Cambridge University Press, Cambridge, 2004).